Journal of Crystal Growth 310 (2008) 3579–3583

Contents lists available at ScienceDirect

Journal of Crystal Growth

journal homepage: www.elsevier.com/locate/jcrysgro

Structure and magnetic properties of CoNiP nanowire arrays embedded in AAO template

Xiaoli He [a,*], Guangbing Yue [a], Yufeng Hao [a], Qiaoling Xu [a], Qing Wei [a], Xiaoguang Zhu [a], Mingguang Kong [a], Lide Zhang, Xing Li [b]

[a] Key Laboratory of Materials Physics, and Anhui Key Laboratory of Nanomaterials and Nanostructures, Institute of Solid State Physics, Chinese Academy of Sciences, Hefei 230031, People's Republic of China

[b] Shanghai Institute of Optics and Fine Mechanics, Chinese Academy of Sciences, Jiading, Shanghai 201800, People's Republic of China

ARTICLE INFO

Article history:
Received 13 November 2007
Received in revised form
10 April 2008
Accepted 16 April 2008
Communicated by J.M. Redwing
Available online 29 April 2008

PACS:
81.07.Bc

Keywords:
A1. Nanostructures
A2. Electrochemical growth
B1. Alloys
B2. Magnetic materials

ABSTRACT

Ternary CoNiP nanowire (NW) arrays have been synthesized by electrochemical deposition inside the nanochannels of anodic aluminum oxide (AAO) template. The CoNiP NWs deposited at room temperature present soft magnetic properties, with both parallel and perpendicular coercivities less than 500 Oe. In contrast, as the electrolyte temperature (T_{elc}) increases from 323 to 343 K, the NWs exhibit hard magnetic properties with coercivities in the range of 1000–2500 Oe. This dramatic increase in coercivities can be attributed to the domain wall pinning that is related to the formation of Ni and Co nanocrystallites and the increase of P content. The parallel coercivity (i.e. the applied field perpendicular to the membrane surface) maximum as high as 2500 Oe with squareness ratio up to 0.8 is achieved at the electrolyte temperature of 328 K. It has been demonstrated that the parallel coercivity of CoNiP NWs can be tuned in a wide range of 200–2500 Oe by controlling the electrolyte temperature, providing an easy way to control magnetic properties and thereby for their integration with magnetic-micro-electro-mechanical systems (MEMS).

1. Introduction

Demands for the continuous increase in data storage density bring the challenge to overcome physical limits for currently used magnetic recording media [1]. Relatively large coercivity (H_c) and high anisotropy are required for ultra-high storage density to overcome the thermal effects and prevent superparamagnetic limit [2]. Due to the attractive magnetic properties, including high perpendicular magnetic anisotropy, enhanced H_c and giant magnetoresistance, magnetic nanowire (NW) arrays have fascinated scientists for decades [3,4]. So far, magnetic NW arrays of cobalt [5], nickel [6], iron [7,8] and different alloys [9–12] have been explored. Various studies have been carried out on CoNiP ternary alloy films as they exhibit hard magnetic properties [13–20]. Luborsky's experiments with electrodeposited Co and CoNi containing group VA (e.g., P, As, Sb and Bi) and VIB (e.g., W, Mo and Cr) as alloying elements showed that P is the most effective component to increase H_c [21]. These CoNiP films with maximum H_c from about 1000 to 2000 Oe exhibit hexagonal (hcp) crystalline columnar microstructures. The increase in H_c is attributed to the precipitation of a NiP nonmagnetic phase at the grain boundaries, which induces magnetic grain separation and hinders magnetic domain wall motion during magnetization switching [14–16]. However, it has been demonstrated that micro-arrays of CoNiP have higher anisotropy and thus higher H_c, as compared to CoNiP films [18]. Recently, the amorphous CoNiP NW arrays were fabricated by electrochemical process [22,23], but have low H_c about 800 Oe. Thus, it is a challenge to fabricate CoNiP alloy NWs with enhanced H_c and squareness ratio.

In this paper, crystalline CoNiP NW arrays were synthesized by electrochemical deposition inside the nanochannels of anodic aluminum oxide (AAO) template. The maximum parallel coercivity ($H_c^{\parallel}$, when the applied field is parallel to the long axis of NWs, i.e. perpendicular to the sample surface) is increased to 2500 Oe with a high parallel squareness ratio ($M_r/M_s^{\parallel}$) of up to 0.8. More significantly, owing to structural variation, $H_c^{\parallel}$ can be achieved in a wide range of 200–2500 Oe simply by modulating the electrolyte temperature (T_{elc}). Since MEMS devices such as micro-actuators, sensors, micromotors, and frictionless microgears require both hard and soft magnetic materials [22], the modulation of magnetic properties by tuning T_{elc} provides a convenient way for optimizing MEMS devices.

* Corresponding author. Tel.: +86 551 5591465; fax: +86 551 5591434.
E-mail address: xl.he@yahoo.com.cn (X. He).

0022-0248/$ - see front matter © 2008 Elsevier B.V. All rights reserved.
doi:10.1016/j.jcrysgro.2008.04.023

2. Experimental methods

Through-hole AAO templates with nanochannel diameter of 50–70 nm and thickness about 50 μm were prepared by a two-step anodization of high-purity aluminum in 0.3 M oxalic acid solution under 40 V_{DC} at about 10 °C [24,25]. Before the electrodeposition, a thin Au layer was sputtered onto one planar surface side of the AAO template as working electrode, and a graphite electrode acted as anode in a two-electrode system. The electrolytes used in our experiments consist of 0.228 M $NiSO_4 \cdot 6H_2O$, 0.213 M $CoSO_4 \cdot 7H_2O$, 0.037 M $NaH_2PO_2 \cdot 2H_2O$, and 0.748 M NH_4Cl, with the pH value about 4.5 [16]. Two groups of CoNiP NW arrays were synthesized under two series of experimental conditions. The NWs in group I were obtained under room temperature (~288 K) with a different current density (J) of 1.0, 1.5, 2.0, 2.5, 3.0 and 4.0 mA/cm^2, respectively, while the NWs in group II were achieved under the constant J of 1.5 mA/cm^2 at different T_{elc} of 313, 323, 328, 333, 343 and 353 K, respectively.

The CoNiP NW arrays were characterized by using scanning electron microscopy (SEM, Sirion 200) and high-resolution transmission electron microscopy (HR-TEM, JEOL-2010) after dissolving AAO templates in an aqueous solution of 10 wt% NaOH. X-ray diffractometry (XRD, X'Pert Pro MPD) was employed to characterize the phase structures. Room temperature magnetic characterization of CoNiP NW arrays was performed on the physics property measurement system (PPMS-9; Quantum Design), with the applied magnetic field parallel and perpendicular to NW arrays, respectively.

3. Results and discussion

3.1. Morphology and structural characterization

Fig. 1 displays the morphology of the CoNiP NWs in group I obtained at $J = 1.5$ mA/cm^2 under room temperature. As shown in Fig. 1a, CoNiP NWs with length of 25 μm have been achieved. The high magnification SEM image (Fig. 1b) shows that the NWs are smooth with diameters about 60 nm, being in agreement with the channel diameters of AAO template. More observations on other NWs in group I and II (not shown here) reveal that they have similar morphologies.

Fig. 2a presents the TEM image of one of group I CoNiP NWs synthesized at $J = 1.5$ mA/cm^2 and $T_{elc} = 288$ K (room temperature), showing that the NWs have smooth surface and uniform diameter along the axis. The selected area electron diffraction (SAED) pattern on the upper-left corner indicates that the NWs are single crystalline with hexagonal structure and grow along [1 0 0] direction, which is also demonstrated by the HRTEM image inserted on the bottom-right corner. We further investigated other samples in group I, such as CoNiP NWs synthesized at $J = 3.0$ mA/cm^2 and $T_{elc} = 288$ K in Fig. 2b. All NWs are single crystalline with the same growth axis [1 0 0], though more defects are observed in the samples prepared under higher J's (not all given here). A representative TEM image of group II samples (Fig. 2c) demonstrates that the NWs in group II are also smooth and uniform in diameter. The SAED in the corner indicates the polycrystalline structure of the NWs, further confirmed by the HR-TEM image (Fig. 2d) where small crystallites inside the NW can be observed. The component compositions of group I and II NWs are analyzed by EDS, as shown in Fig. 3. Group I NWs are composed primarily of Co (Fig. 3a), and the contents of Co, Ni and P change slightly with the increase of J at room temperature (Fig. 3b). On the other hand, the component contents of group II NWs as a function of T_{elc} are presented in Fig. 3c and d. Interestingly, the Co content decreases sharply from 80 at.% to 10 at.%, and, correspondingly, the content of Ni increases rapidly from 10 at.% to 80 at.%. Due to comparatively higher P co-deposition with Ni than with Co [17], it is reasonable that the P content has a relatively large increase from about 3 at.% to 18 at.% with the T_{elc} changing from 288 to 353 K.

X-ray diffraction patterns of the NWs are shown in Fig. 4. The peak in Fig. 4a corresponding to hcp-Co (1 0 0) implies that group I samples have the preferred hcp [1 0 0] orientation, whereas (see Fig. 4b) there exists a peak at 44.8° corresponding to hcp-Co (0 0 2) or fcc-Ni (1 1 1) in group II NWs. Namely, the preferred orientation of CoNiP varies when T_{elc} increases to higher temperature.

Combining the above results of TEM, SAED, EDS and XRD, we propose that group I NWs are Ni and P dissolved hcp-Co matrix with preferential [1 0 0] growth direction. By additionally considering that alloying element P tends to concentrate at the grain boundaries in alloys [26] and the structure of Ni–P matrix embedded with Co nanocrystallites was found previously [27], we infer that group II NWs with relatively large P content are mixed Ni and Co nanocrystallites and P atoms gather at their grain boundaries, and the amount ratio of these two kinds of nanocrystallites is larger than 4:1.

3.2. Magnetic properties

It is well known that the benefits found in nanostructural alloys stem from their chemical and structural variations on a nano-scale, which is important for optimizing MEMS devices. Here, the magnetic properties of the two groups of CoNiP NWs having different structures were investigated, as shown in Fig. 5. In addition, the dependences of H_c (the solid lines) and Mr/Ms (the dashed lines) of group I and II NWs on J and T_{elc} are also given in Fig. 6. The symbols "∥" and "⊥" represent that the external field is parallel and perpendicular to the long axis of NWs, respectively.

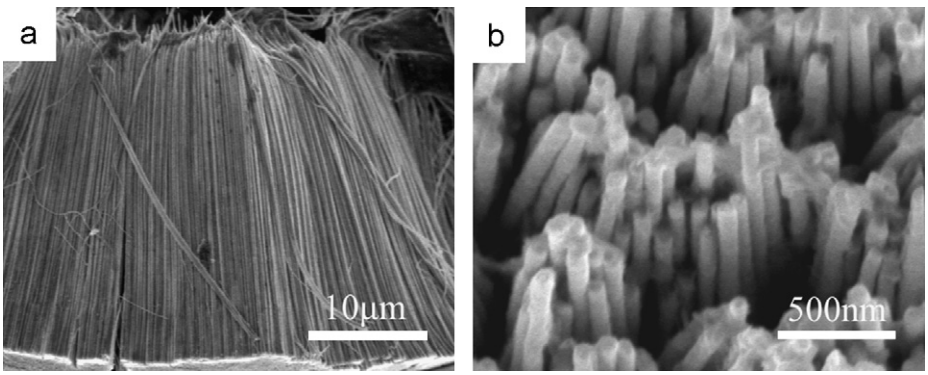

Fig. 1. SEM images of CoNiP NW arrays obtained under $J = 1.5$ mA/cm^2 and $T_{elc} = 288$K: (a) low magnification side view image; (b) high magnification top view image.

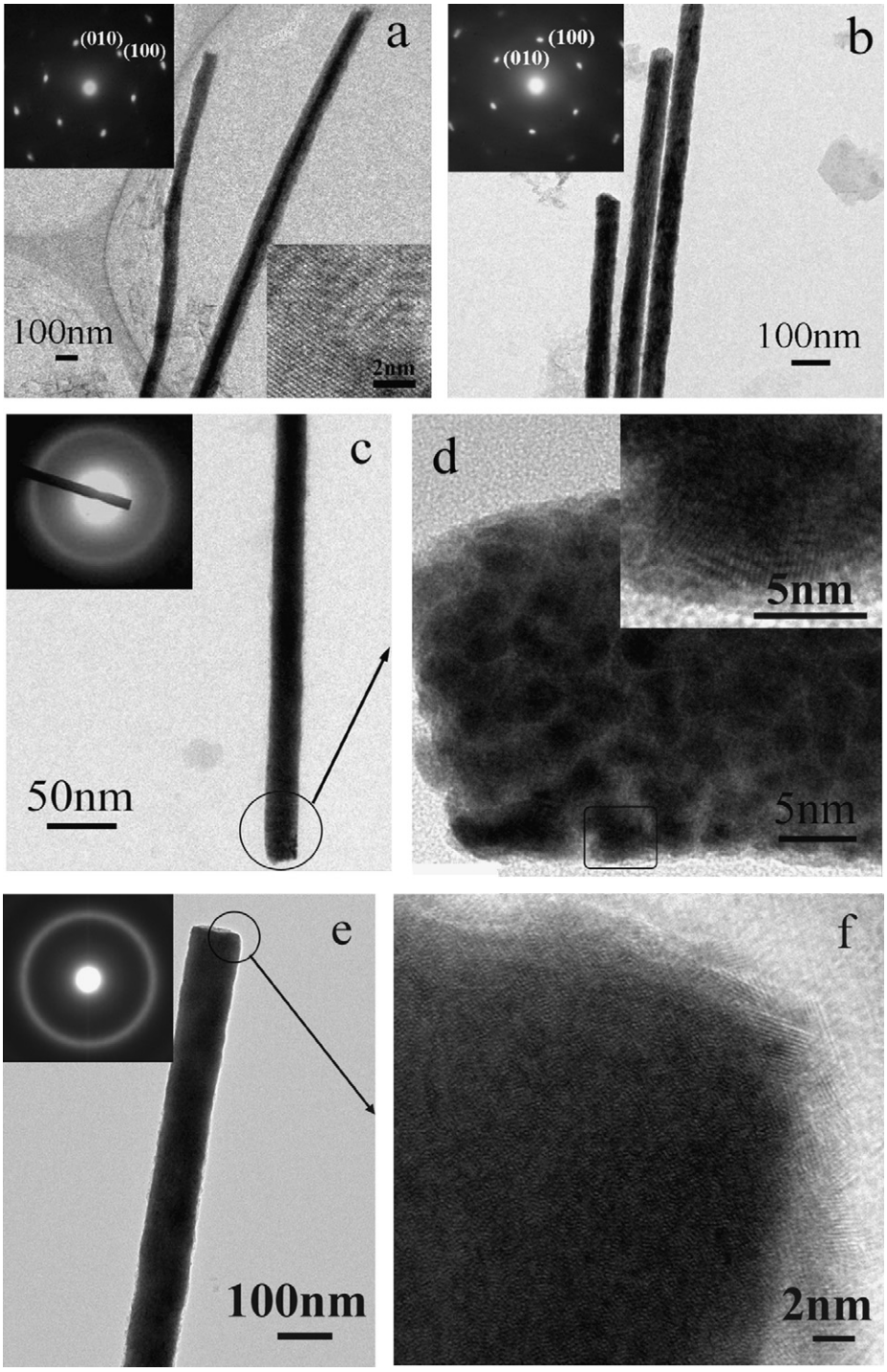

Fig. 2. TEM images of CoNiP NWs. (a) NWs in group I obtained under $J = 1.5\,mA/cm^2$ and $T_{elc} = 288\,K$, with the SAED pattern on the upper-left corner and a lattice-resolved image on the bottom-right corner; (b) NWs in group I obtained under $J = 3.0\,mA/cm^2$ and $T_{elc} = 288\,K$, the inset is the corresponding SAED pattern; (c) a single NW in group II obtained under $J = 1.5\,mA/cm^2$ and $T_{elc} = 328\,K$, with the SAED pattern on the corner; (d) a lattice-resolved image of the CoNiP NW taken from the circular area marked in (c), the inset is a higher magnification TEM image of the area marked with a pane, revealing the crystalline structure of the nanograins; (e) a NW in group II obtained under $J = 1.5\,mA/cm^2$ and $T_{elc} = 353\,K$ with the SAED pattern on the corner; (f) a lattice-resolved image of the NW taken from the circular area marked in (e).

Fig. 5a–c displays the magnetic hysteresis loops of three kinds of CoNiP NW arrays in group I achieved under J of 1.5, 2.5 and $4.0\,mA/cm^2$, respectively. Minor differences exist in magnetic properties among these samples and all these NWs possess relatively narrow hysteresis loops and small magnetic anisotropy. Comparatively low H_c (lower than 500 Oe) and low squarenesses (lower than 0.4) are observed, as seen in Fig. 6a. The maximum H_c ($H_c^{\parallel} = H_c^{\perp} = 484\,Oe$) is obtained at $J = 2.5\,mA/cm^2$ with the maximum $M_r/M_s^{\parallel}$ and $M_r/M_s^{\perp}$ of 0.38 and 0.24, respectively. The soft magnetism may be related to the single crystal hcp microstructure.

From Fig. 5d–f, it can be seen that the magnetic properties of group II NW arrays vary with T_{elc}. The solid lines in Fig. 6b depict the plot graph of $H_c^{\parallel}$ and $H_c^{\perp}$ of group II NWs versus T_{elc}. By comparison, we note that $H_c^{\parallel}$ is always larger than $H_c^{\perp}$, but they have the same variation tendency. At 288 K, the $H_c^{\parallel}$ and $H_c^{\perp}$

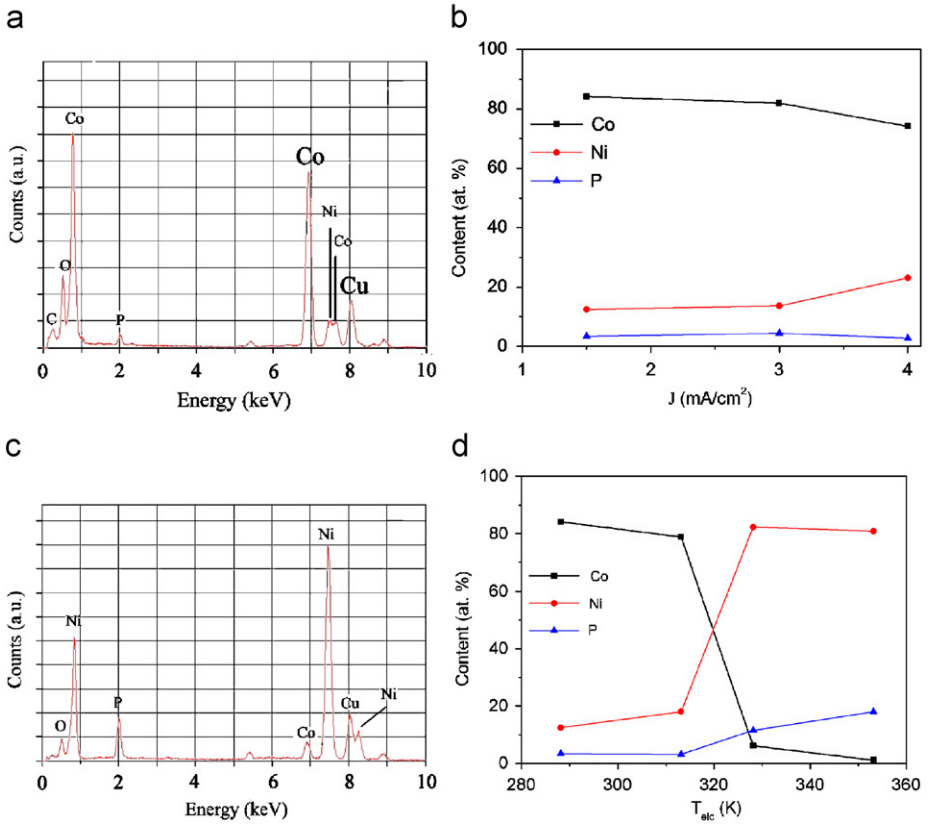

Fig. 3. (a) Representative EDS spectrum of CoNiP NWs obtained under $J = 1.5\,mA/cm^2$ and $T_{elc} = 288\,K$ for group I and (b) the dependence of component composition of group I NWs on J; (c) representative EDS spectrum of NWs fabricated at $J = 1.5\,mA/cm^2$ and $T_{elc} = 328\,K$ for group II and (d) the dependence of component composition of group II NWs on T_{elc}.

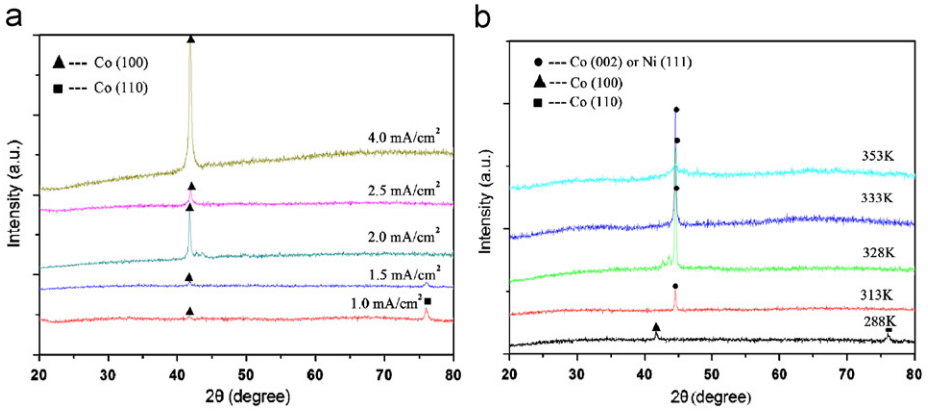

Fig. 4. XRD patterns of (a) group I CoNiP NW arrays at $T_{elc} = 288\,K$; (b) group II at $J = 1.5\,mA/cm^2$.

have a close minimum value of about 200 Oe, which then increase dramatically with T_{elc} and separately reach the maximum value ($H_c^{\parallel} = 2500$ Oe, $H_c^{\perp} = 2150$ Oe) at 328 K. As the T_{elc} increases further to 353 K, both decrease sharply to 325 and 197 Oe, respectively. In other words, the $H_c^{\parallel}$ and $H_c^{\perp}$ have high values (1000–2500 Oe) in the T_{elc} range of 323–343 K, while as T_{elc} goes beyond the range weaker H_c in two directions lower than 500 Oe will be induced. Moreover, it can also be seen that $H_c^{\parallel}$ and $H_c^{\perp}$ of group II NWs have large differences at $T_{elc} = 323$–343 K, which is suitable for perpendicular magnetic recording. On the other hand, as seen from the dashed lines in Fig. 6b, both $M_r/M_s^{\parallel}$ and $M_r/M_s^{\perp}$ increase dramatically with the increase of T_{elc}. When the T_{elc} reaches the range of 323–343 K, both values achieve the maximum of 0.7–0.8 and 0.25–0.38, respectively. It should be noted that the difference between them is also very large in this T_{elc} range and reaches the largest value of 0.64 at $T_{elc} = 343$ K, where $M_r/M_s^{\parallel} = 0.80$ and $M_r/M_s^{\perp} = 0.14$. Such difference decreases and both values are close to 0.4 when the T_{elc} increases further to 353 K. The reason of magnetism behavior for this group samples is also discussed. Firstly, group II NWs are Ni-rich (about 80 at.%) polycrystalline NWs with preferential grain orientations of hcp (0 0 2) and fcc (1 1 1) texture. The stronger shape anisotropy compared with magnetocrystalline anisotropy [8,28] ensures the large squareness in group II CoNiP NWs. On the other hand, with the elevation of T_{elc} from room temperature, the increasing P atoms concentrate at the grain boundaries in NWs and help the

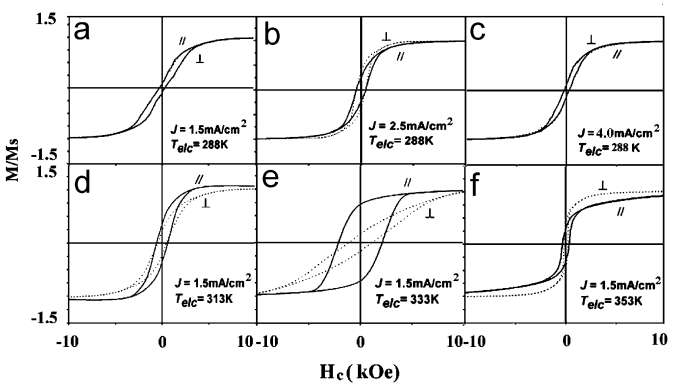

Fig. 5. a, b, and c are hysteresis loops of group I CoNiP NWs in AAO template obtained at $T_{elc} = 288$ K and different J of 2.0 mA/cm^2 (a); 2.5 mA/cm^2 (b) and 4.0 mA/cm^2 (c); d, e and f are magnetic curves of group II NWs achieved under the same current density of 1.5 mA/cm^2 and at different temperatures of 313 K (d); 333 K (e) and 353 K (f). The symbols of "∥" and "⊥" represent the external field parallel and perpendicular to the long axis of NWs, respectively.

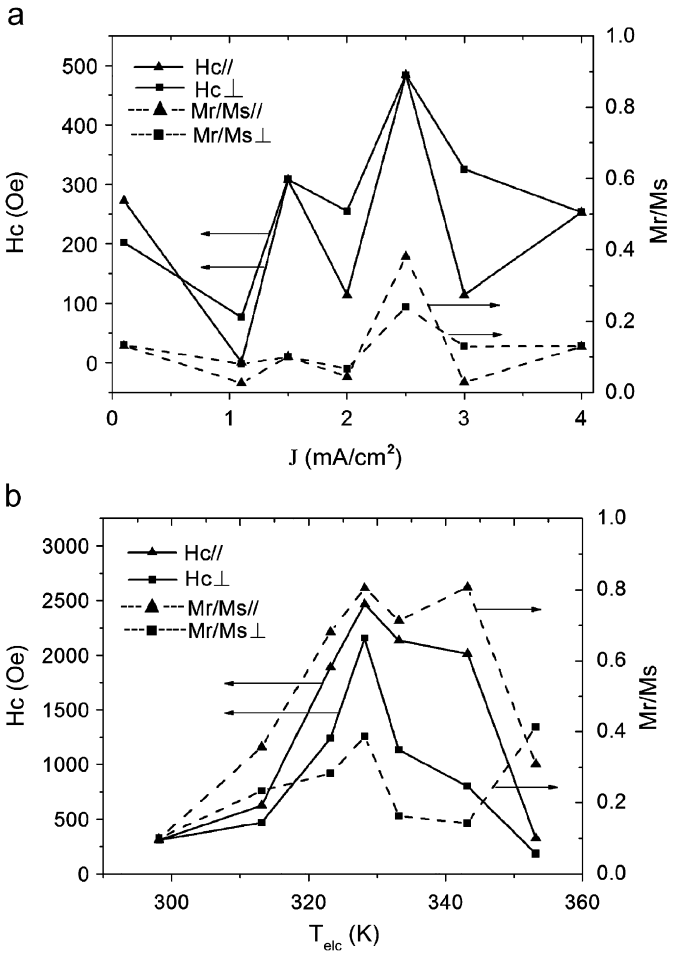

Fig. 6. Dependences of H_c and Mr/Ms of (a) group I CoNiP NW arrays on J, and (b) group II NW arrays on T_{elc}. "∥" and "⊥" represent the external field parallel and perpendicular to the long axis of NWs, respectively.

formation of domain wall pinning, which consequently enhances the overall H_c. However, in a solution of even higher temperature (more than 343 K), group II NWs exhibit very fine grain structures and even tend to be amorphous due to an excess in the P content, contributing to the soft magnetic properties of the samples.

4. Conclusions

CoNiP NW arrays were synthesized by electrodeposition inside the nanochannels of AAO templates, and the corresponding structure and magnetic properties were characterized. The results indicate that the magnetic properties strongly depend on the component contents and crystal structures of CoNiP NWs, which can be controlled by T_{elc}. In the T_{elc} range of 323–343 K, the synthesized CoNiP NWs are polycrystalline embedded with Co and Ni nanocrystallites and have hard magnetism ($H_c^{\parallel} \sim 1000$–$2500$ Oe and $M_r/M_s^{\parallel} \sim 0.8$) with large magnetic anisotropy. These NWs with large H_c and M_r/M_s are expected to have important application as hard magnetic materials in MEMS. On the other hand, under room temperature, the synthesized NWs are monocrystalline Co matrix doped with Ni and P and have soft magnetic properties with low H_c (less than 500 Oe) and low M_r/M_s (less than 0.4). These kinds of NWs have potentials as soft magnetic materials in MEMS. In addition, our experimental method provides an easy way to realize the control of magnetic properties, which thereby favor their integration in MEMS.

Acknowledgment

We are grateful for the support of the Natural Science Foundation of China (Grant nos. 50525207 and 10374092) and National Basic Research Program of China (Grant no. 2007CB936601).

References

[1] Adam Lapicki, Kyongha Kang, Takao Suzuki, IEEE Trans. Magn. 38 (2002) 2589.
[2] Diane Ung, Guillaume Viau, Christian Ricolleau, Fabienne Warmont, Patrick Gredin, Fernand Fievet, Adv. Mater. 17 (2005) 338.
[3] C.Z. Wang, G.W. Meng, Q.Q. Fang, X.S. Peng, Y.W. Wang, Q. Fang, L.D. Zhang, J. Phys. D: Appl. Phys. 35 (2002) 738.
[4] Y.W. Wang, L.D. Zhang, G.W. Meng, X.S. Peng, Y.X. Jin, J. Zhang, J. Phys. Chem. B 106 (2002) 2502.
[5] A. Kazadi Mukenga Bantua, J. Rivas, J. Appl. Phys. 89 (2001) 15.
[6] A. Kumar, S. Fahler, H. Schlorb, K. Leistner, L. Schultz, Phys. Rev. B 73 (2006) 064421.
[7] P.M. Paulus, F. Luis, M. Kroll, G. Schmid, L.J. de Jongh, J. Magn. Magn. Mater. 224 (2001) 180.
[8] M. Kroll, W.J. Blaua, D. Grandjeanb, R.E. Benfieldb, F. Luisc, P.M. Paulusc, L.J. de Jonghc, J. Magn. Magn. Mater. 249 (2002) 241.
[9] T.R. Gao, L.F. Yin, C.S. Tian, M. Lu, H. Sang, S.M. Zhou, J. Magn. Magn. Mater. 300 (2006) 471.
[10] Q.T. Wang, G.Z. Wang, X.H. Han, X.P. Wang, J.G. Hou, J. Phys. Chem. B 109 (2005) 23326.
[11] D.S. Xue, J.L. Fu, H.G. Shi, J. Magn. Magn. Mater. 308 (2007) 1.
[12] Y. Dahmane, L. Cagnon, J. Voiron, S. Pairis, M. Bacia, L. Ortega, N. Benbrahim, A. Kadri, J. Phys. D: Appl. Phys. 39 (2006) 4523.
[13] D.M. Kirkwood, G. Pattanaik, G. Zangari, J. Electrochem. Soc. 154 (2007) D363.
[14] C. Byun, G.C. Rauch, D.J. Young, C.A. Klepper, J. Appl. Phys. 73 (1993) 15.
[15] N. Fenineche, A.M. Chaze, C. Coddet, Surf. Coat. Technol. 88 (1996) 264.
[16] D.Y. Park, N.V. Myung, M. Schwartz, K. Nobe, Electrochim. Acta 47 (2002) 2893.
[17] T.S.N. Sankara Narayanan, S. Selvakumar, A. Stephen, Surf. Coat. Technol. 172 (2003) 298.
[18] S. Guan, B.J. Nelson, J. Electrochem. Soc. 152 (2005) C190.
[19] R.N. Emerson, C.J. Kennady, S. Ganesan, Thin Solid Film 515 (2007) 3391.
[20] H. Chiriac, A.E. Moga, M. Urse, I. Paduraru, N. Lupu, J. Magn. Magn. Mater. 272 (2004) 1678.
[21] F.E. Luborsky, IEEE Trans. Magn. 6 (1970) 502.
[22] H. Chiriac, A.E. Moga, C. Gherasim, CAS 2005 Proc. 1 (2005) 59.
[23] X.Y. Yuan, G.S. Wu, T. Xie, Y. Lin, G.W. Meng, L.D. Zhang, Solid State Commun. 130 (2004) 429.
[24] H. Masuda, M. Satoh, Jpn. J. Appl. Phys. 35 (1996) 1126.
[25] Y. Li, G.W. Meng, L.D. Zhang, F. Phillipp, Appl. Phys. Lett. 76 (2000) 2011.
[26] N.V. Myung, D.-Y. Park, B.-Y. Yoo, P.T.A. Sumodjo, J. Magn. Magn. Mater. 265 (2003) 189.
[27] D.N. Lee, K.H. Hur, Scr. Mater. 40 (1999) 1333.
[28] M. Zheng, R. Skomski, Y. Liu, D.J. Sellmyer, J. Phys.: Condens. Matter 12 (2000) L497.